Geologic heterogeneity recognition using discrete wavelet transformation for subsurface flow solute transport simulations

Hussein Mustapha [a,b,*], Snehamoy Chatterjee [a,c], Roussos Dimitrakopoulos [a], Thomas Graf [d]

[a] COSMO–Stochastic Mine Planning Laboratory, Department of Mining and Materials Engineering, McGill University, Montreal, Canada
[b] Schlumberger, United Kingdom
[c] National Institute of Technology Rourkela 769008, India
[d] Institute of Fluid Mechanics in Civil Engineering, Leibniz Universität Hannover, Hannover, Germany

A B S T R A C T

Subsurface flow and solute transport simulations are performed using different scenarios of permeability fields generated from the sequential Gaussian simulation method (SGS), the multiple-point FILTERSIM algorithm and a new multiple-point wavelet-based simulation method (SWS). The SWS method is a multiple-point pattern-based simulation method which uses discrete wavelet transformation for the representation of geologic heterogeneity. For pattern-based simulation, patterns are generated by scanning a training image with a spatial template. The pattern classifications were performed after reducing the dimension of patterns by wavelet decomposition at the suitable scale and by taking only scaling components of wavelet decomposed patterns. The simulation is performed in a sequential manner by finding the best-matched class corresponding to the conditioning data and by randomly sampling a pattern from the best-matched class. The developed method is compared with two other multi-point simulation algorithms, FLTERSIM and SIMPAT. The comparative results revealed that the proposed method is computationally faster than the other two methods while the simulation maps are comparable. Numerical simulations of two flow problems are performed using SGS, SWS and FILTERSIM realizations. The numerical results show a superiority of the SWS method over SGS and FILTERSIM in terms of reproduction of the reference images main features, and agreement with flow and transport results obtained on reference images.

© 2012 Elsevier Ltd. All rights reserved.

1. Introduction

The development and application of geostatistical methods for modeling geologic heterogeneity exist in a variety of engineering and geoscience fields [5,9,11,13,15,16,18–20,22,23,32,35,39,40, 42,44,46,48,51,53,54,61,68,72,76], and the use of these applications have become common practice. Second-order spatial statistics and the geological information they contain remains the mainstream modeling paradigm from the past four decades. Several investigations have assumed a multivariate log-normal distribution for the hydraulic conductivity (K), and have used a Gaussian model [1,6,25,63–65,75]. Although second-order statistics are adequate for the complete statistical description of Gaussian processes, they are inadequate for modeling geological phenomena which typically deviate from Gaussianity and exhibit complex spatial patterns. These concerns have been articulated

since the 1990s [36,42,73]. If the effectiveness of geostatistical modeling, particularly in the presence of non-Gaussianity and non-linearity, is to be enhanced, more spatial information needs to be extracted from measurements and made available. This vital information enhances modeling applications such as the prediction and quantification of spatial uncertainty. Enhancing modeling and predictive capabilities have major applied implications, as demonstrated in reservoirs/aquifers; complex spatial arrangements of permeable and impermeable units drive the production characteristics of the reservoir/aquifers, and predictions from drilling and seismic data have major economic implications. One can certainly expand this list with examples from underground storage of hazardous waste, environmental modeling, ground water resources, CO_2 sequestration in geological formations [43,47], and so on.

Several previous studies explored the effect of simulation algorithms or heterogeneity conceptual models on the spatial distribution of hydrogeologic parameters and consequent flow responses. A thorough discussion and details are provided in [2,3,30,33,41,42,46,62,66,70,74,76–78,81], which are briefly reiterated herein. In the previous works, comparisons between spatial patterns generated by the various methods including

---

* Corresponding author at: Department of Mining and Materials Engineering, McGill University, Montreal, Canada.
E-mail addresses: hussein.mustapha@mcgill.ca, hmustapha.math@gmail.com (H. Mustapha).

multi-Gaussian model, indicator simulation, simulated annealing technique, and a Markov chain model show significant differences in spatial distributions. Gaussian, Truncated Gaussian, and Sequential Indicator simulation methods are also used to generate a deep-sea fan system in the pore volume geometry connection and up-scaled permeability, and comparisons have been drawn. It is also shown that, after up-scaling, large scale permeability distribution was sensitive to the geostatistical model used. The previous studies, extensively discussed in [46,78], show that flow and transport response functions are strongly affected by the choice of the model. For example, Gomez-Hernandez and Wen [30] have compared a Gaussian model and three alternatives that have the same Gaussian histogram and covariance function but with different spatial continuity for extreme values. The results showed that different connected patterns in K values are produced by each alternative. Lee et al. [46] showed significantly different flow simulation results generated with two sets of statistically equivalent geostatistical conditional simulations in 3D: one being an indicator method that emphasizes fairly strong organization of hydrofacies [25,26], the other being a standard Gaussian random field method [21,31]. In Ref. [46], it is shown that important geologic characteristics may not be captured by a spatial covariance model, even if that model is exhaustively determined and closely fits the exponential function.

Today's trends, developments and applications focus on the so-called multiple point simulation algorithms, such as the SNESIM [67], FILTERSIM [79,81], and SIMPAT [4] algorithms and related extensions [8,12,52]. Additionally related new developments include Markov random field based multipoint type approaches [14,73], and kernel approaches [63], as well as multi-scale simulations based on discrete wavelet decomposition [10,29]. Recently, HOSIM [56–57] introduced a new point-based multiple-point (mp) simulation algorithm based on high order spatial cumulants. The algorithm has successfully been applied to underground flow and solute transport simulations, and has been found superior to other multiple-point algorithms [59]. HOSIM algorithm employs a high-dimensional Legendre series to approximate the conditional probability densities. The number of coefficients in the series varies with respect to the number of samples used to calculate a value at a given point, and to the order of the series. In 1D, for a series of order n, the number of coefficients to be calculated is of order $O(n)$; in 2D, it is of order $O(n^2)$. Using m samples and a series of order n, the conditional probability density calculation involves a number of coefficients of order $O(n^m)$. The calculation of these coefficients at every point is time consuming, and storing them also requires significant memory. In addition, the number m of samples, found in a neighborhood of a point, increases gradually through the conditional simulation process. Thus, the algorithm may significantly slowdown the CPU time for large-scale problems. In the best cases, HOSIM has been found much slower than FILTERSIM method. Finally, the algorithm works only for continuous images, and calculating cross-cumulants will lead to slower algorithm.

As an alternative, the present paper proposes an efficient pattern-based simulation algorithm of continuous and categorical images using discrete wavelet transformation. Some comparisons with FILTERSIM showed that the proposed method is more accurate and faster.

The pattern database is generated in a manner similar to other mp simulation techniques and is classified by using the scaling coefficients of the wavelet decomposition of each pattern. The main difference of a wavelet-based approach from other multipoint algorithms is how the pattern database is classified. The scaling coefficients of a wavelet decomposed pattern can capture most of the pattern variability, and at the same time reduce the dimensionality of the pattern database. Pattern database classification is performed using scaling coefficients of patterns and by applying the k-means clustering technique. The class is represented by class prototype. For simulation, the similarity of the class prototype with the conditioning data event is calculated. A random pattern is generated from the 'best match' class.

In this paper, a novel method based on discrete wavelet transformation is presented. The developed method is an alternative to the multiple-point methods discussed above. The performance of the proposed wavelet-based method was compared with two other multi-point algorithms, FILTERSIM and SIMPAT. Effects of spatial geologic heterogeneity - generated by the SWS, SGS and FILTERSIM methods - on flow and transport simulation results are also studied.

2. Simulation of geologic heterogeneity using discrete wavelet transformation

The proposed method consists of five steps (described below in detail): (1) generation of a pattern database, (2) dimensional reduction of the pattern database using discrete wavelet transformation, (3) classification of the pattern database, (4) similarity measures between conditional data and class prototypes during simulation, and (5) sequential pattern-based simulation. The same terminologies as other multi-point simulation algorithms [4,67,79,80] are used in this paper.

2.1. Generation of a pattern database

Pattern-based simulation is an image reconstruction problem [5,79,80], which reproduces the multiple-point characteristics of a training image as captured by the template used. A training image (TI) is an analog of the geological architecture deemed present in the field/reservoir. In pattern-based simulation, the training image patterns are reproduced in a stochastic manner, which ultimately respects the multi-point relations of the training image as captured by the template(s) used [4]. Pattern-based simulation algorithms imply two steps: (1) the generation of a pattern database; and (2) searching for the best match pattern from the pattern database to the conditioning data. Define $ti(\mathbf{u})$ as a value of the training image ti where $\mathbf{u} \in G_{ti}$ and G_{ti} is the regular Cartesian grid discretizing the training image, $ti_T(\mathbf{u})$ indicates a specific multiple-point vector of $ti(u)$ values within a template $\mathbf{T}$ centered at node $\mathbf{u}$, that is

$$ti_T(\mathbf{u}) = \{ti(\mathbf{u} + \mathbf{h}_1), ti(\mathbf{u} + \mathbf{h}_2), \ldots, ti(\mathbf{u} + \mathbf{h}_\alpha), \ldots, ti(\mathbf{u} + \mathbf{h}_{nT})\}. \quad (1)$$

Where, the $\mathbf{h}_\alpha$ vectors are the vectors defining the geometry of the n_T nodes of template $\mathbf{T}$ and $\alpha = \{1, 2, \ldots, n_T\}$. The vector $\mathbf{h}_1 = 0$ represents the central location $\mathbf{u}$ of template $\mathbf{T}$.

Same as for other multi-point algorithms [4,67,79,80], the pattern database, $patdb_T$, is then obtained by scanning ti using template $\mathbf{T}$ and stored using the multi-point $ti_T(\mathbf{u})$ vectors in the database.

Patterns, in the pattern database $patdb_T$, are location-independent, and kth pattern is presented as

$$\mathbf{pat}_T^k = \{pat^k(\mathbf{h}_1), pat^k(\mathbf{h}_2), \ldots, pat^k(\mathbf{h}_\alpha), \ldots, pat^k(\mathbf{h}_{nT})\}. \quad (2)$$

Where, $k = 1, 2, \ldots, n_{Pat_T}$, n_{Pat_T} is number of patterns in the pattern database, and $pat^k(\mathbf{h}_1), pat^k(\mathbf{h}_2), \ldots, pat^k(\mathbf{h}_\alpha), \ldots, pat^k(\mathbf{h}_{nT})$ are values obtained from $ti_T(\mathbf{u})$.

During the simulation, the best matched pattern corresponding to conditional multi-point data will be searched from the pattern database. Since, the number of patterns (n_{Pat_T}) in the pattern database is very large, to search the best matched pattern from the pattern database is computationally demanding. To reduce the computational time of simulation, FILTERSIM and other pattern base multipoint simulation algorithms, classify the entire pattern database into a number of classes. For simulation, the distance
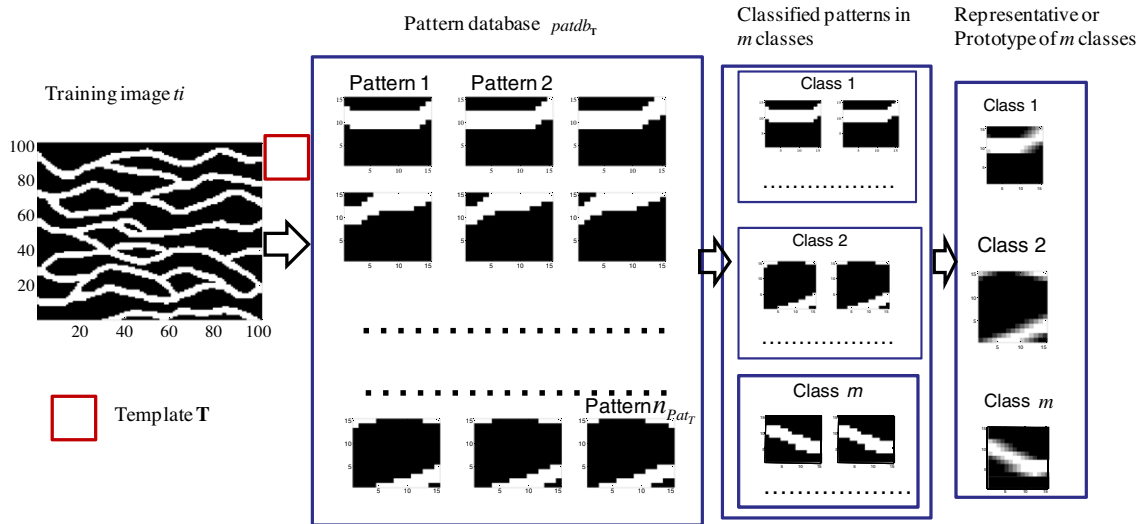
Fig. 1. Basic steps involved from pattern generation to class representation.
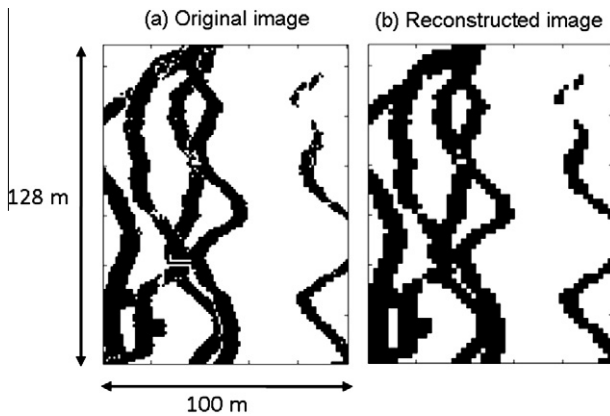

Fig. 2. (a) Original image considered as a large pattern; and (b) its reconstructed image after reducing 75% of the data of the original image.

from the conditioning data to the class is calculated. Therefore, representatives (prototypes) of each class are calculated from each class. Fig. 1 represents the basic steps involved from pattern generation to class representation in pattern-based multi-point simulation algorithm.

To generate the pattern database $patdb_{\mathbf{T}}$, a template size $\mathbf{T}$ must be selected. An automatic template-selection algorithm as presented by Honarkhah and Caers [37] is applied in this paper for selecting the template size.

2.2. Dimensional reduction of a pattern database

After generating the $patdb_{\mathbf{T}}$, the classification of the pattern database will be performed so that during simulation, instead of searching the entire pattern database ($patdb_{\mathbf{T}}$), only some representative members, i.e. prototypes of the classes, are compared with the conditioning data event as shown in Fig. 1. However, when the template dimension is large, the dimension of $patdb_{\mathbf{T}}$ will also be large. Therefore, classification of this large dimensional pattern database $patdb_{\mathbf{T}}$ is a computationally demanding task. In previous research, the $patdb_{\mathbf{T}}$ classification was performed by reducing the dimensions of the pattern by using filters [75,76]. In Refs. [75,76], 6 and 9 filters are used for two- and three-dimensional

training images, respectively. The main limitations of the filter-based dimensional reduction technique are (a) it is always difficult to represent a complex patter only using a few filter values, and there is no guarantee that those filter values will successfully represent a pattern; and (b) the filter based method does not show any theoretical or numerical proof of the amount of data variability of patterns represented by filter values. A wavelet-based representation of patterns is introduced where the dimension of the pattern-for-pattern classification can be reduced by selecting the scale of wavelet decomposition. The term scale is referred to here as the resolution or support size on which a given wavelength of a TI or analog is defined. In the context of spatial simulation, a solution for developing methods that facilitates the explicit reproduction of consistent complex scale relationships between patterns has been proposed for two-dimensional cases based on the use of the discrete wavelet transformation (DWT), as detailed in [29]. It is noted that the main difference between the proposed method and FILTERSIM method is how the patterns of the pattern database are classified.

Wavelet analysis can decompose any pattern into a series of orthogonal basis functions [49]. Multi-resolution wavelet analysis is performed according to scale – thus decomposing data into different datasets according to scale – and provides both frequency and spatial information. A two-dimensional dataset can be considered as a square integrable function in Hilbert space. Due to its multi-resolution property, the wavelet function provides a series of orthonormal bases functions by scaling and shifting the original basis function, known as the mother wavelet function. The two-dimensional DWT is a decomposition of a dataset in terms of a set of scaled and shifted wavelet functions $\{\psi^{LH}, \psi^{HL}, \psi^{HH}\}$ and scaling functions ϕ^{LL} that form an orthonormal basis for square integrable Hilbert space $L^2(\Re^2)$ [17]. The DWT of a two-dimensional pattern $ti_{\mathbf{T}}$ of $N \times N$ can be decomposed as

$$ti_{\mathbf{T}}^k = \sum_{i,l=0}^{N_J-1} a_{J,i,l}^k \, \phi_{J,i,l}^{LL} + \sum_{B \in D} \sum_{j=1}^{J} \sum_{i,l=0}^{N_j-1} w_{j,i,l}^{k,B} \psi_{j,i,l}^B, \tag{3}$$

where $D = \{LH, HL, HH\}$, $N_j = N/2^j$, J is number of scale, and $k = 1, 2, \ldots, n_{Pat_T}$. The functions included in set D are known as wavelet sub-bands. The two-dimensional DWT is an extension of the one-dimensional DWT in two different directions, due to the separable properties of the wavelet basis function [17]. Two-dimensional wavelets can be constructed by taking the product of a
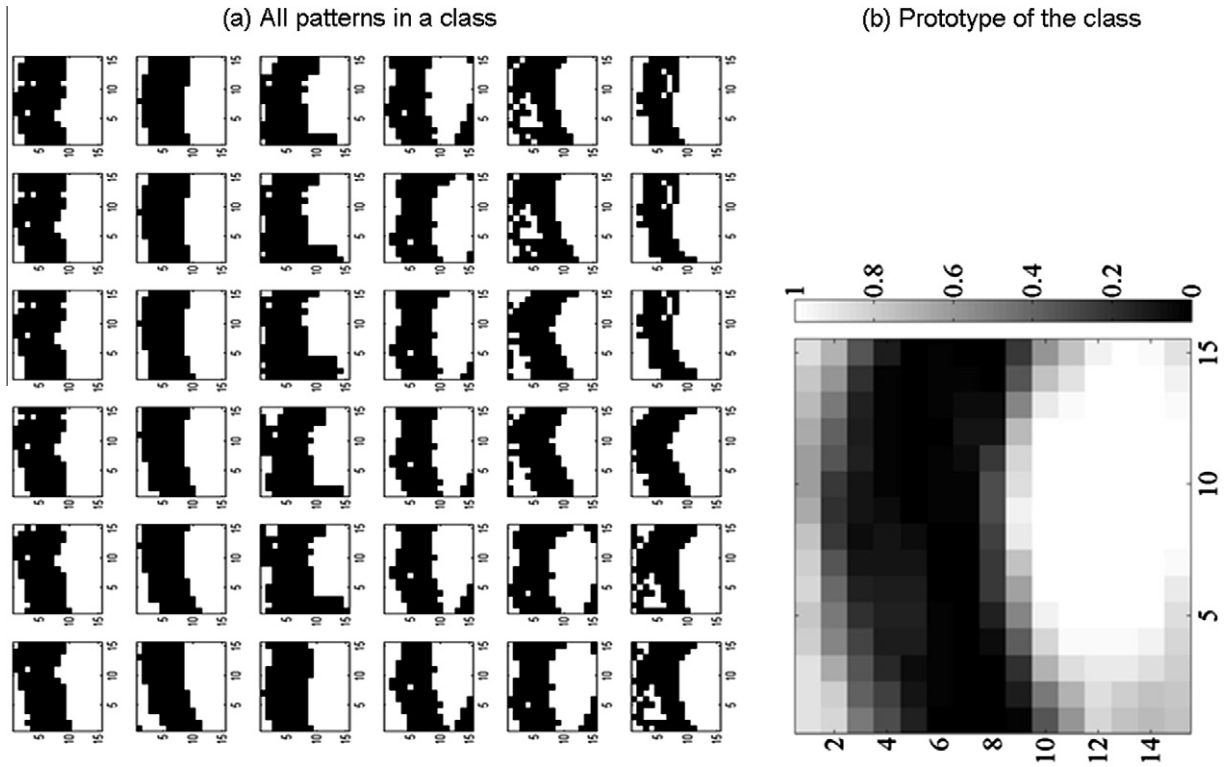
Fig. 3. All 36 patterns in a class after pattern classification of the pattern database in (a); and (b) a prototype of the class in (a).

one-dimensional scaling or wavelet in the x direction and a one-dimensional scaling or wavelet in the y direction. The two-dimensional scaling and wavelet function can then be written as follows

$$
\begin{aligned}
\phi^{LL}(x,y) &= \phi^L(x)\phi^L(y), \\
\psi^{LH}(x,y) &= \psi^L(x)\phi^H(y), \\
\psi^{HL}(x,y) &= \psi^H(x)\phi^L(y), \\
\psi^{HH}(x,y) &= \psi^H(x)\psi^H(y),
\end{aligned}
\tag{4}
$$

where, ϕ^L and ψ^H are one-dimensional scaling and wavelet functions, respectively.

The scaling and wavelet coefficients a_{j-1} and w_{j-1} at scale $j-1$ can be experimentally calculated by taking inner products [17]

$$
\begin{aligned}
a_{j-1} &= \langle ti_T, \phi_j \rangle, \\
w_{j-1}^B &= \langle ti_T, \psi_j^B \rangle.
\end{aligned}
\tag{5}
$$

In this paper, the Haar wavelet basis functions are used [49]. For Haar wavelet, $\phi(x)$ and $\psi(x)$ are presented as [47]

$$
\psi^H(x) = \begin{cases} 1 & 0 \leqslant x < \frac{1}{2} \\ -1 & \frac{1}{2} \leqslant x < 1 \\ 0 & \text{otherwise} \end{cases}, \quad \phi^L(x) = \begin{cases} 1 & 0 \leqslant x < 1 \\ 0 & \text{otherwise} \end{cases}.
\tag{6}
$$

The scaling image of the pattern $a_{J,i,l}$ provides average type information about the pattern and preserves most of the data variability; thus one can easily calculate the amount of data variability captured by a scaling image of a certain scale decomposition of a pattern [49]. It is noted that the size of the scaling image $a_{J,i,l}$ is $N_j \times N_j$, where $N_j = N/2^j$, $j = 1, 2, \ldots, J$, and J is number of scale. Therefore, the amount of data in a scaling image is 2^{j*d} times less than the amount of data in a pattern ti_T, where d is the dimension of patterns. Hence, if only the scaling image of the patterns in the pattern databases are used for classification, the computational

time can substantially be reduced depending upon the scale of decomposition.

For an example, Fig. 2(a) is considered as a large pattern. The reconstructed pattern is presented in Fig. 1(b) by keeping only the scaling image $a_{J,i,l}$ after one scale decomposition. It is observed that the pattern reproduces the original pattern well, at the same time reducing 75% of the data of the original pattern.

The main concern of the wavelet-based simulation is the selection of the appropriate scale of decomposition. In this paper, we have applied the singular value decomposition (SVD) method. The SVD facilitates the selection of a global natural scale in DWT. The natural scale is the level associated with the most dominant eigenvalue. The eigenvector corresponding to the dominant eigenvalue is considered the optimal scale [60]. To know more about the optimum scale selection by eigenvector decomposition, readers are requested to follow [60].

2.3. Pattern database classification

For classification of pattern database $patdb_T$, the scaling image of the patterns $a_{J,i,l}$, (which is reduced in dimension depending on the value of J) is used. The k-means clustering technique [24,36,38] is applied to classify the pattern database $patdb_T$. The k-means clustering technique divides the $patdb_T$ into a predefined number of classes such that the sum of the inter-class distance is maximized. In k-means clustering algorithm, the $patdb_T$ is classified based on the selected priory cluster number (m). The algorithm is initialized by selecting m random patterns from the $patdb_T$. These selected m patterns represent the initial class centroids. Since the $patdb_T$ classification is performed using only the scaling image of patterns $a_{J,i,l}$, randomly selected scaling images of m patterns from $patdb_T$ act as initial centroids. The aim of the k-means clustering algorithm is to minimize the following objective function iteratively

$$P = \sum_{s=1}^{m} \sum_{k=1}^{n_{Pat_T}} \left\| a_{J,i,l}^k - c_s \right\|^2, \tag{7}$$

where, $\left\| a_{J,i,l}^k - c_s \right\|^2$ is the squared Euclidian distance between a scaling image of a pattern $a_{J,i,l}^k$ and the centroids of class c_s, is a measure of the distance of the n_{Pat_T} patterns from their respective cluster centers.

After classifying the $patdb_T$ by minimizing the objective function at Eq. (7), prototypes of classes are calculated. The prototype is the representative member of each class. These prototypes are used during the simulation process, when the similarity between the conditional data event and prototype class is calculated. The prototype value is obtained by averaging all patterns falling into a particular class after classification. Fig. 1 shows the patterns, pattern classification and their prototypes.

To select the optimal cluster number, we have used gap statistics as presented by Tibshirani et al. [71]. Suppose that we have clustered the data into k clusters $c_1, c_2, \ldots, c_k$, with C_r denoting the indices of observation in cluster r, and $n_r = |C_r|$. If D_r is the sum of the pairwise Euclidian distances for all points in cluster r, then

$$W_k = \sum_{r=1}^{k} \frac{1}{2n_r} D_r. \tag{8}$$

The optimal number of clusters is then the value of k for which the gap value is maximum. The gap value for k can be defined as

$$\text{gap}_n(k) = E_n\{\log(W_k)\} - \log(W_k), \tag{9}$$

where E_n denotes the expected value of sample size n from the reference distribution. The reference vectors are obtained by generating uniform sampling over the range of the values for that feature. For more details about the reference vector generation, interested readers can consult [71].

To show the efficacy of the proposed classification algorithm using only the wavelet decomposed scaling image $a_{J,i,l}$ of patterns

and k-means clustering algorithm, Fig. 2(a) is considered as a two-category training image. A template size, which is optimally selected, of 15×15 is used to extract patterns from the training image. The scale of decomposition is selected by SVD method and the optimum scale is 2 in this case. The scaling image after two-scale wavelet decomposition is used for $patdb_T$ classification.

The optimum cluster number is selected by observing the gap statistics and it was observed that 71 is the optimum cluster in this problem. Fig. 3 represents all patterns (36) in a particular class after classification of $patdb_T$ using the proposed approach. It is observed from the figure that the patterns look very similar, and the algorithm can easily classify the patterns. Since the pattern classification was performed using the scaling image $a_{J,i,l}$ after two scale decomposition, the dimensionality of the patterns are reduced from 225 (15×15) to 16 (4×4, size of scaling image after two scale decomposition). Since the dimensions are reduced from 225 to 16, it can easily be concluded that the proposed algorithm will be computationally faster than classifying patterns based on their original dimensions.

2.4. Similarity measures between conditional data and class prototypes

After classifying the $patdb_T$ and prototype calculation, simulation of spatial patterns was initiated. During simulation, the similarity between the conditioning data event and the prototypes of the classes were carried out. A sequential simulation algorithm [30] is used for pattern-based simulation in this paper. At each visited node, a conditioning data event is obtained by placing the same template used in the training image, centering at the node to be simulated. The similarity between the conditioning data and prototypes of classes are calculated by a distance function. A distance function is used to calculate the distance from the prototypes of classes to the conditioning data event. The distance function used in this paper is L^2-norm [10,32,45]. The distance function used is
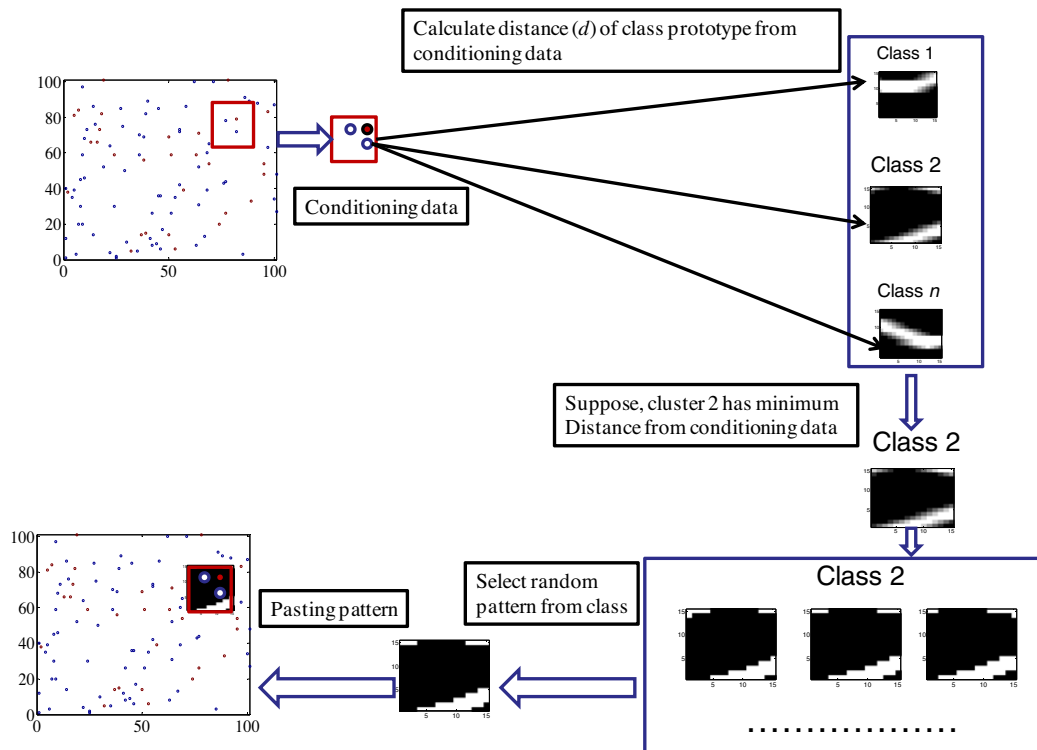

Fig. 4. Schematic diagram of the simulation method proposed in this paper.
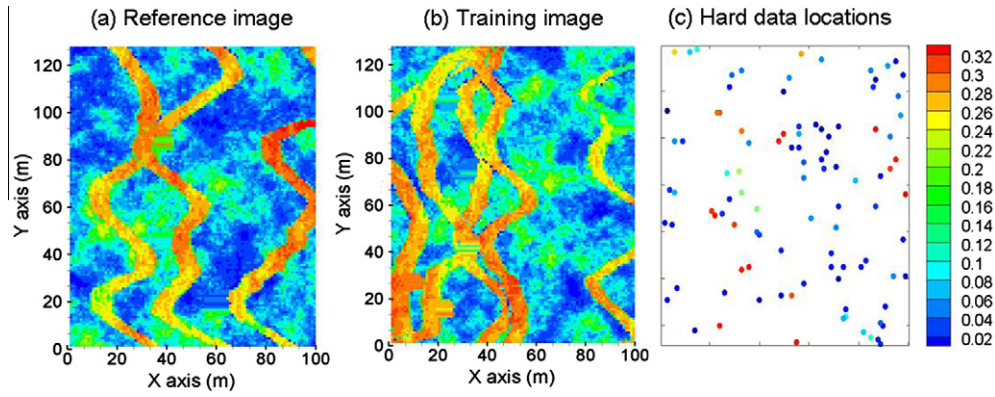
Fig. 5. Reference image obtained from a 3D fluvial reservoir (a); (b) a training; and (c) 208 hard data set generated randomly from the reference image to be simulated.

$$d = \sum_{i=1}^{nT} (\overline{pat}^s(\mathbf{h}_i) - y(\mathbf{h}_i))^2, \qquad (10)$$

where, $y(\mathbf{h}_i)$ is the conditioning data event and $\overline{pat}^s(\mathbf{h}_i)$ is the prototype of class s, If some of $y(\mathbf{h}_i)$ values are missing in the conditioning data, those $\mathbf{h}_i$ will not be considered for distance calculation.

When simulating a node, if all the nodes within a template are known, i.e. $y(\mathbf{h}_i)$ values are available for all $\mathbf{h}_i$, the distance calculation with a large template will be computationally demanding. To reduce the computational time of a distance calculation, a scaling image of the wavelet decomposed conditioning data can be used. The modified distance function can be presented as

$$d = \sum_{i=1}^{N_j \times N_j} (\overline{a}_{j,i,l}(\mathbf{h}_i) - a_{j,i,l}^y(\mathbf{h}_i))^2, \qquad (11)$$

where, $N_j \times N_j$ is the number of data in the scaling image after wavelet decomposition, $\overline{a}_{j,i,l}(\mathbf{h}_i)$ is the scaling image of $\overline{pat}^s(\mathbf{h}_i)$, and $a_{j,i,l}^y$ is the scaling image of $y(\mathbf{h}_i)$.

If within the conditioning data event any hard data are present, Eq. (10) will be used for distance calculation even if all the nodes within a template are fully known.

2.5. A general algorithm

Fig. 4 presents the schematic diagram of the simulation method proposed in this paper. The main steps of the proposed method are as follows:

1. Scan the training image using the selected template **T**. Perform wavelet decomposition of the generated patterns using the selected scale.
2. Classify the pattern database $patdb_\mathbf{T}$, based on only the scaling image by an optimally selected cluster number and calculate the classes prototypes.
3. Define a random path visiting once and only once all unsampled nodes.
4. Places the template **T** at each unsampled location u to get conditioning data. The distances from the class prototypes are calculated from the conditioning data available within the template using Eq. (10), (11). Select the class which has minimum distance from the conditioning data. If no conditioning data are available within **T**, a random class is selected.
5. Draw a random pattern from the selected class and paste the pattern by centering the simulated point u. If any hard conditioning data are present in any node within the template of u, they are frozen before pasting the selected pattern.
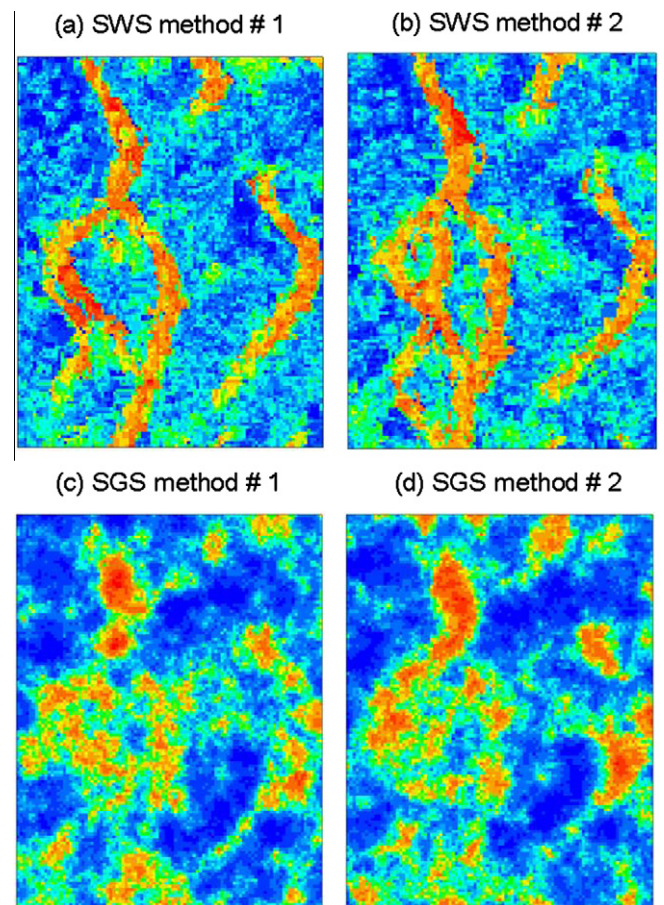6. Repeat Steps 4 and 5 for the next points in the random path defined in Step 3.

Fig. 6. Two simulated realizations generated using both the SGS method and the proposed method (SWS). (# 1) and (# 2) refer to realization number.

7. Repeat Steps 3–6 to generate different realizations using different random paths.

3. Numerical models

Two-dimensional continuous horizontal slices of a 3D fluvial reservoir are used as reference images to perform numerical simulations using realizations generated by the SGS, SWS and FILTERSIM methods. The SWS method is compared, in particular, to the SGS and FILTERSIM methods for the following reasons: (1) all three methods can perform simulations on continuous and categorical images, (2) the FILTERSIM method is an mp pattern-based
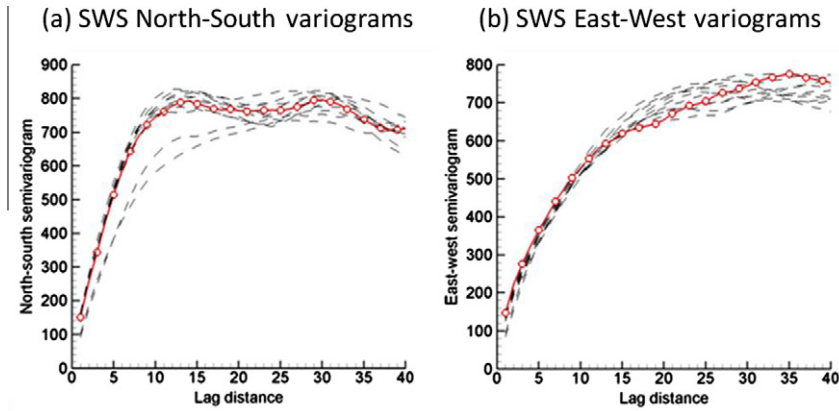
Fig. 7. North–South (a) and East–West (b) variograms of SWS realizations. The circles refer to the data set and the solid lines refer to the realizations.
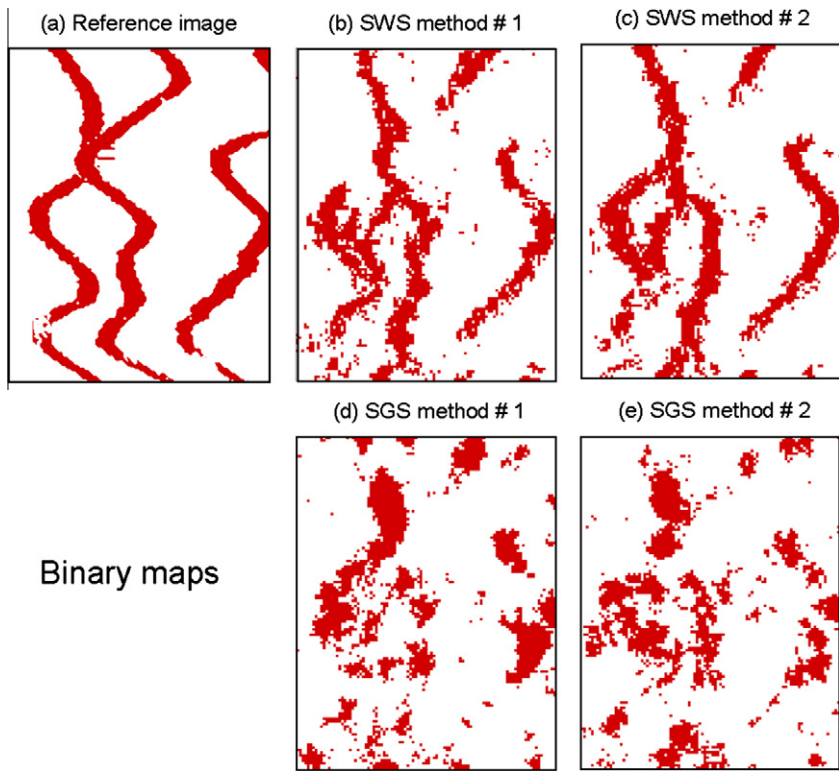

Fig. 8. Binary maps, with value 1 if $K > 85\%$ and 0 otherwise, for the reference image (a), two realizations of SWS method (b,d) and SGS method (c,e), respectively.

simulation algorithm, which uses a classification method of spatial patterns, and (3) the SGS is a well-known two-point statistical method.

The data sets used here (Fig. 5) are obtained from the Stanford V Reservoir Data Set [50]. Stanford V is a synthetic fluvial reservoir data set containing different channel thicknesses and orientations. A conductivity (K) field lumps the conductivity distribution at different thicknesses, and is shown in Fig. 5(a). Fig. 5(a) is the first reference image used in the following numerical analysis, and a second reference image is used later for a detailed comparison between SWS and FILTERSIM.

K-field represents the reference image to be simulated using sample data sets. The data set is randomly generated with 208 samples (Fig. 5(c)) and is combined with a training image to generate the pattern database. The training image, shown in Fig. 5(b), is another horizontal section of the 3D reservoir. All the images used have the dimensions of 100×128 cells in x- and y-direction, respectively, with uniform node spacing of 1 m in each direction.

Table 1
Computing times for SIMPAT, FILTERSIM and our proposed method (SWS).

	Computing time (s)
SIMPAT	6373
FILTERSIM	2135
SWS	1232

We generated 10 realizations of the conductivity field for each stochastic simulation. Realizations of SWS, SGS and FILTERSIM are compared by studying their impacts on underground flow and solute transport. Several flow simulation problems are used including an incompressible two-phase problem, and a single-phase problem of advective–dispersive–diffusive solute transport. The governing equations of the flow and solute transport problems are not repeated here however for more detail we refer to [7].
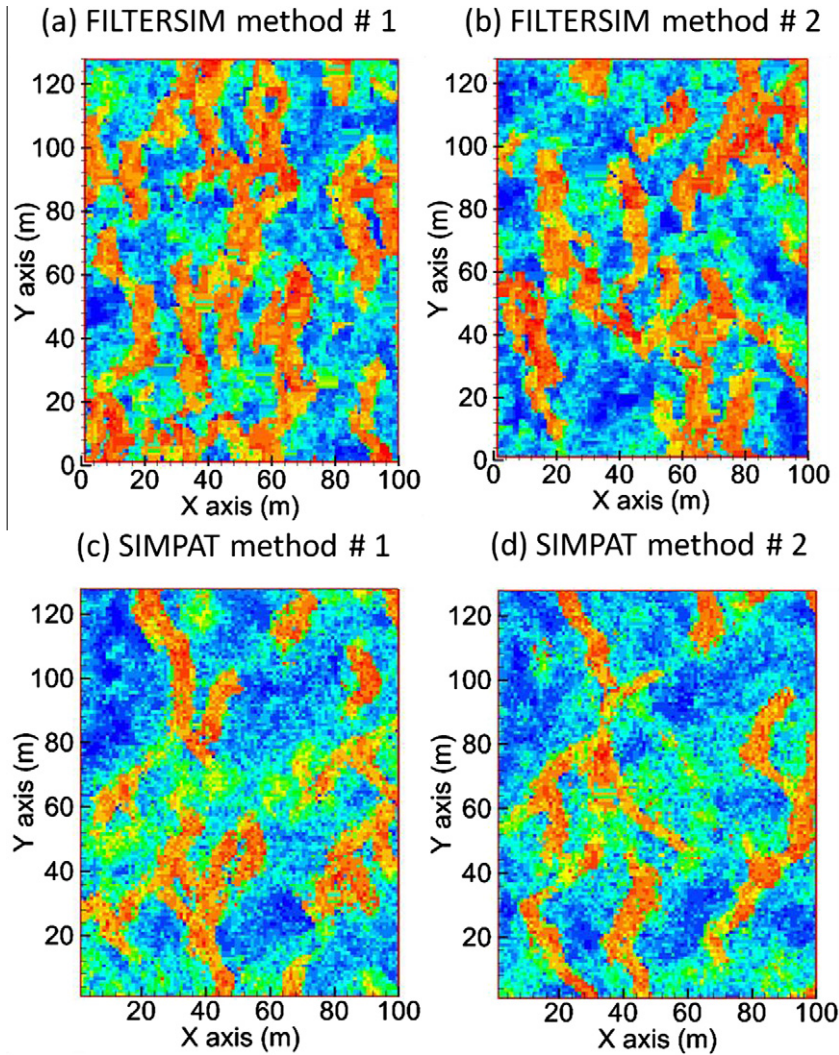
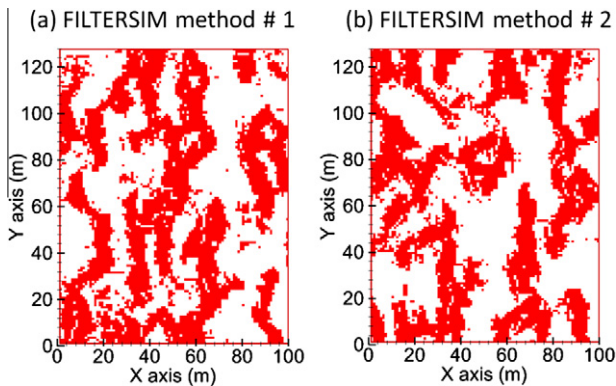Fig. 9. Conditionally simulated realizations using the FILTERSIM (a,b) and SIMPAT (c,d) methods.

Fig. 10. Binary maps, with value 1 if $K > 85\%$ and 0 otherwise, for two realizations of the FILTERSIM method.
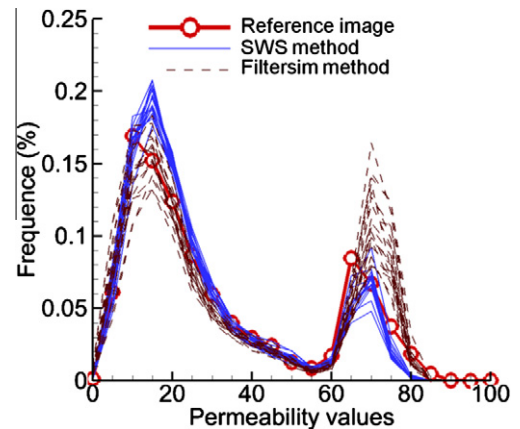

Fig. 11. Histograms of the SWS and FILTERSIM realizations. The circles refer to the data set and the solid and dashed lines refer to the SWS and FILTERSIM realizations, respectively.

4. Results and discussion

4.1. Geostatistical simulations

In this section, we compare the SWS proposed method to both the two-point SGS method and to the multiple-point FILTERSIM and SIMPAT methods.

4.1.1. Comparative study with two-point SGS method

Different realizations are generated by the proposed SWS and SGS methods. Two different realizations of each method are shown in Fig. 6. This figure shows a much better reproduction of the
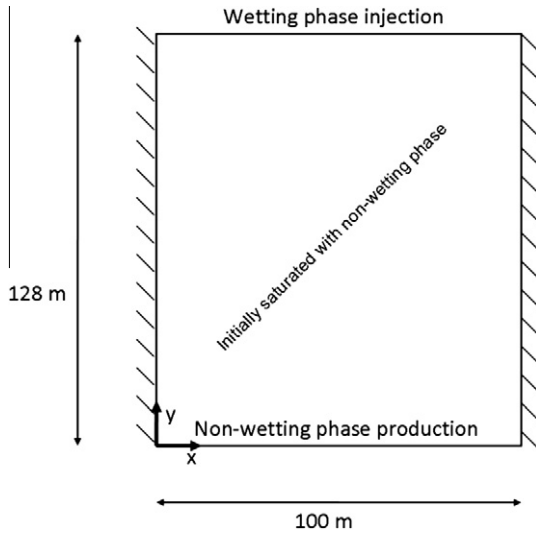
Fig. 12. A conceptual model for incompressible two-phase flow simulation problem. The domain is initially saturated by a non-wetting phase, i.e. oil. Wetting phase, i.e. water, is injected from the top to produce non-wetting phase from the bottom.

complex spatial patterns and large-scale spatial features using the proposed method rather than SGS.

The proposed method's realizations better preserve the spatial structure of channels, and they are in good agreement with the data as well as reference image. The SGS realizations lack much of the high-K channeling. In addition, SWS realizations preserve the statistics of the data as shown first by Fig. 7. This figure shows the comparison between SWS realization variograms along East–West and North–South directions of the data set. Connectivity of

Table 2

Model parameters used for the analysis of two-phase problem; ϕ, k denotes, respectively, the matrix porosity and permeability. S_a, ρ_a, k_{ra} and μ_a are the saturation, density, relative permeability, and viscosity of phase α (α = wetting phase and non-wetting phase), respectively.

Domain dimensions:	100 m × 128 m
Rock properties:	$\phi = 0.2$; $k = [9.86\text{E}{-}13 \text{ m}^2; 9.86\text{E}{-}11 \text{ m}^2]$
Fluid properties:	$\mu_w = 1$ cP; $\mu_n = 0.45$ cP; 1 cP $= 10^{-3}$ kg/ms;
	$\rho_w = 1000$ kg/m^3; $\rho_n = 660$ kg/m^3
Relative perm abilities:	Quadratic: $k_{rw} = S_e^2$; $k_{rn} = (1 - S_e)^2$;
	$S_e = (S_w - S_{rw})/(1 - S_{rw} - S_{rn})$ the normalized saturation
Residual saturations:	$S_{rw} = 0$; $S_{rn} = 0$
Mesh size:	12 573 rectangles
PVI:	Pore volume injection
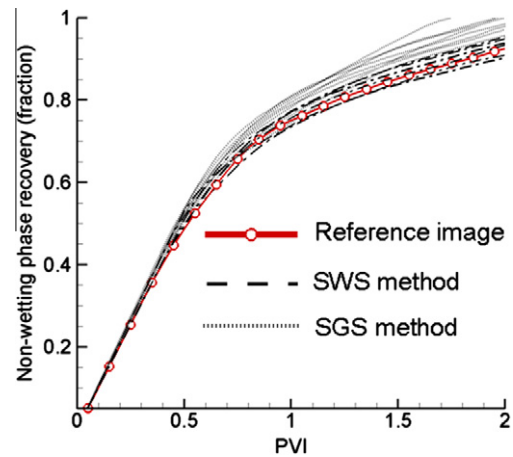
Fig. 14. Recovery of the non-wetting phase vs. Pore volume injection (PVI) for both the proposed method SWS and SGS method realizations. The continuous line with circles refers to the recovery in the reference domain.
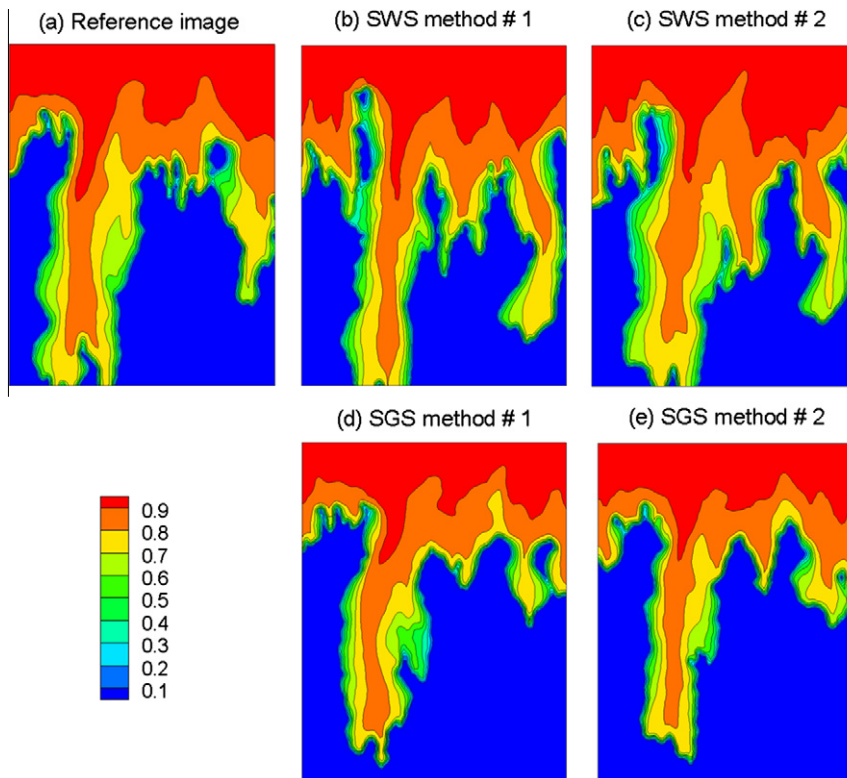
Fig. 13. Wetting-phase saturation profiles at 0.5 pore volume injection (PVI) in the reference image (a), two realizations of SWS method (b,d) and SGS method (c,e). Color scale represents water saturation. (For interpretation of the references to color in this figure legend, the reader is referred to the web version of this article.)

Table 3
Model parameters used for the analysis of solute transport problem.

| Parameter	Value
Free-solution diffusion coefficient	1×10^{-9} m^2 s^{-1}
Water density	1000 kg m^{-3}
Water viscosity	1.1×10^{-3} kg m^{-1} s^{-1}
Specific storage of matrix	9.96×10^{-5} m^{-1}
Matrix permeability	[9.86E−13 m^2; 9.86E−11 m^2]
Matrix longitudinal dispersivity	1.0 m
Matrix transverse dispersivity	0.1 m
Matrix porosity	0.2
Tortuosity	0.1

both the SWS and SGS methods is checked through the spatial connection of the upper 15% high-permeability values. Fig. 8 shows the binary map obtained (1 if $K > (0.85 * (max_K - min_K) + min_K)$ and 0 otherwise) for the reference image, SWS and SGS methods. As a result, SWS produces much better connected channels than SGS and the connectivity is consistent with the result obtained in the reference image.

4.1.2. Comparative study with other multiple-point methods

In this section, the wavelet based method (SWS) is compared to the multiple-point FILTERSIM and SIMPAT methods. A template
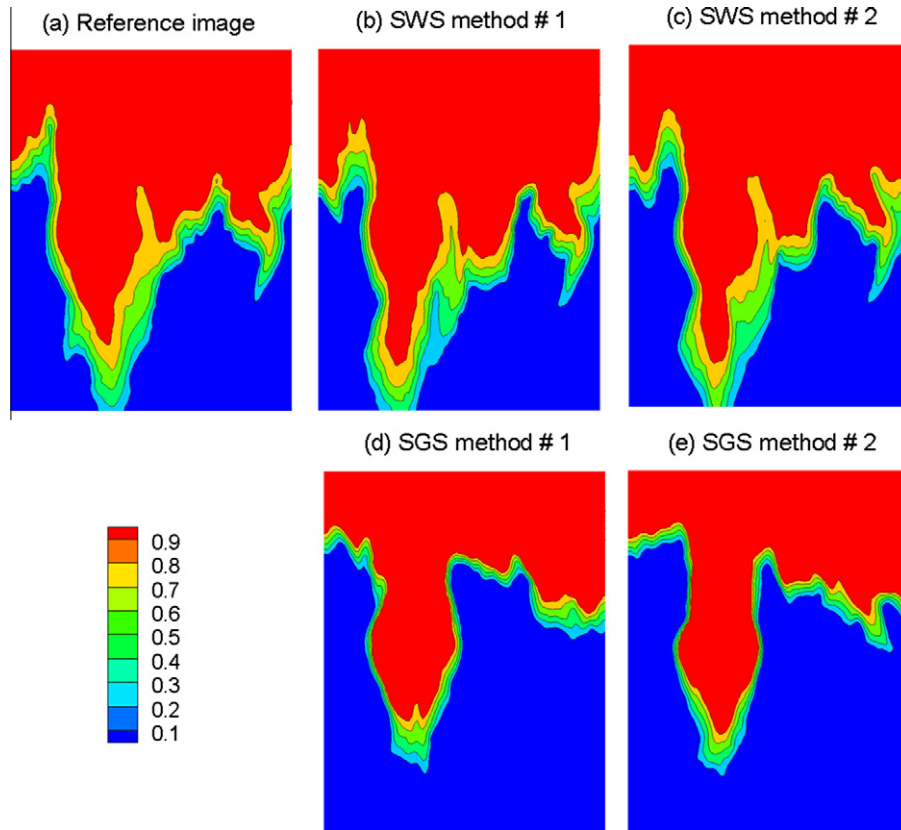
Fig. 15. Solute transport simulation in reference image (a), proposed method SWS (b,d) and SGS (c,e) method realizations. Time = 50 000 days. Color scale represents relative solute concentration C/C_0. (For interpretation of the references to color in this figure legend, the reader is referred to the web version of this article.)
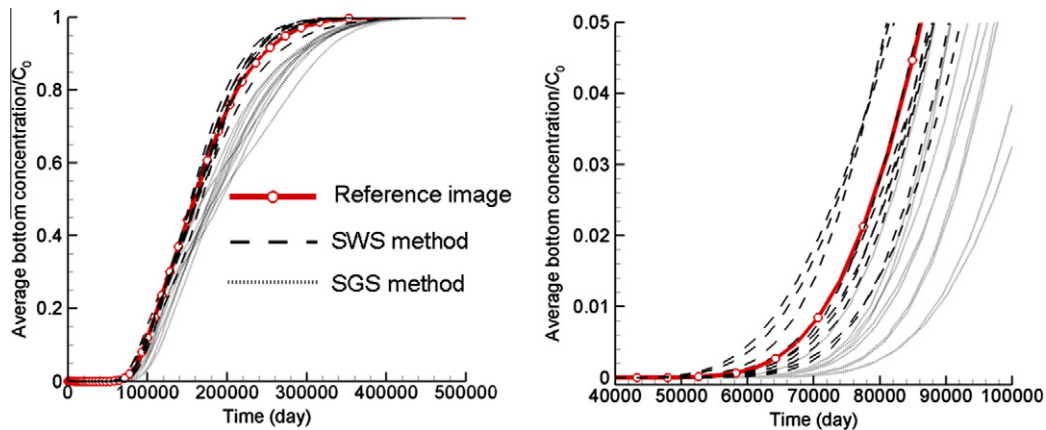
Fig. 16. Average concentration along the bottom boundary vs. time for both the proposed method SWS and SGS method realizations; the continuous line with circles refers to the concentration in the reference domain (left). A close-up is shown in on the right.

size is selected using an automatic template-selection algorithm [37]. The optimum scale is 13×13 in this case. The template coefficients are extracted by moving the template over the training image and storing the extracted patterns in the training database. For conditional simulation, the wavelet decomposition is performed after generating the pattern database to reduce the dimensionality.

The critical step of wavelet decomposition for dimensionality reduction is the selection of the optimal scale. The optimum scale selected by SVD method [60] is 3. The k-means clustering technique is utilized to classify the database and therefore reduce the computation time required for searching the patterns within. The number of clusters is selected by calculating the gap statistics
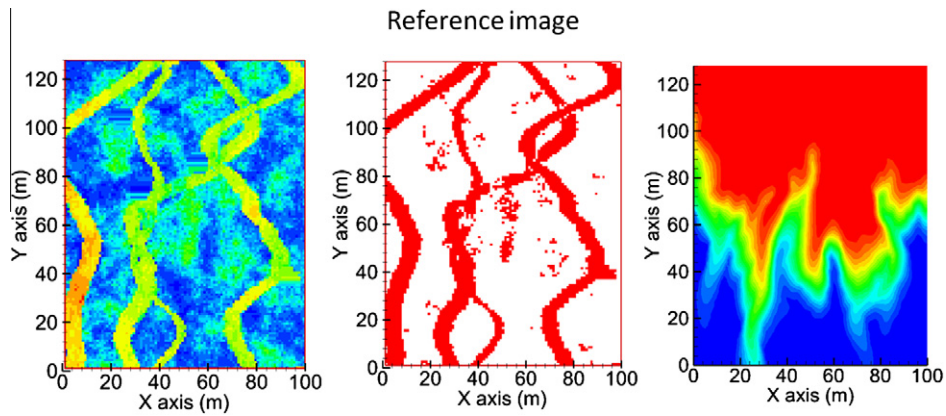

Fig. 17. A second reference image (a) close to the training image in Fig. 5(b); (b), and (c) are, respectively, the binary map, with value 1 if $K > 85\%$ and 0 otherwise, and the solute transport simulation in reference image (a).
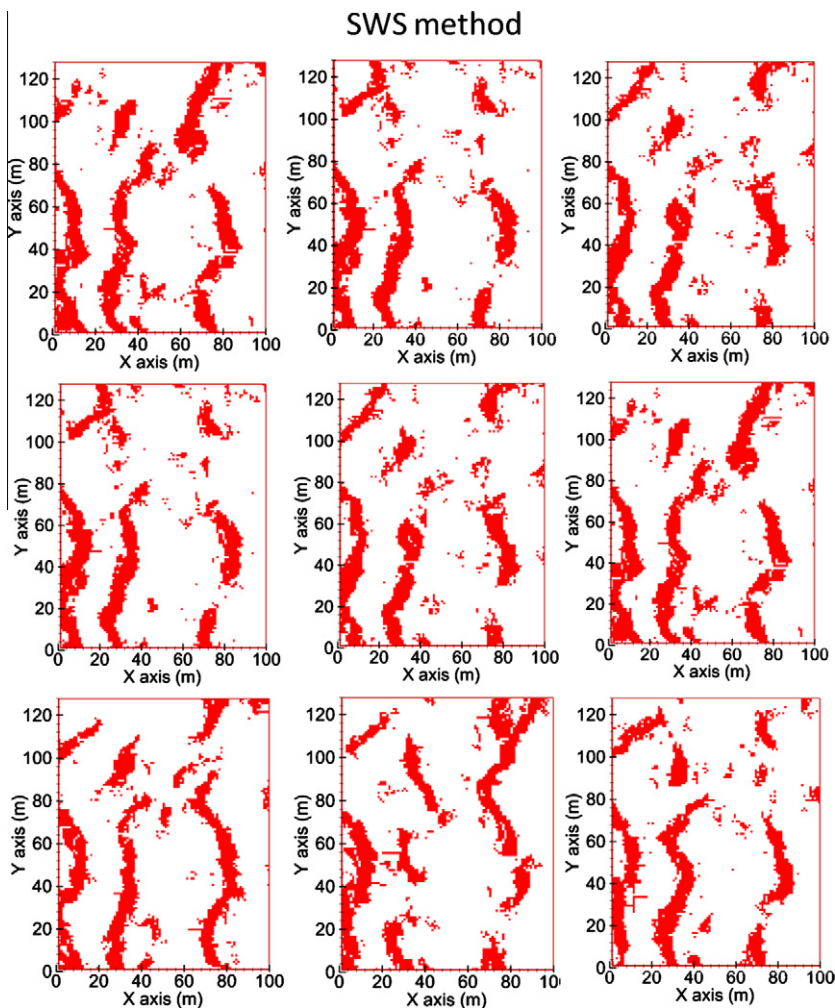

Fig. 18. Binary maps, with value 1 if $K > 85\%$ and 0 otherwise, for 9 new realizations of the SWS method simulating the spatial patterns in Fig. 18(a) using the training image in Fig. 5(b).

[71]. The gap statistic value is maximum when the cluster number is 84; therefore, the cluster number of 84 is the optimal cluster number for this example. To assess the performance of the proposed wavelet-based simulation method, a comparative study is performed in terms of computing time as well as simulated realizations with both the SIMPAT [4] and FILTERSIM [75,76] algorithms. All three algorithms were tested under the MATLAB environment. The same random path, training image, and conditioning data were used in all three algorithms. For both SIMPAT and FILTERSIM algorithms the template size is optimally selected and the optimum template is 13 × 13. The cluster number in our approach is optimally selected as discussed previously and optimum cluster number is 84. The cluster number for the FILTERSIM algorithm is 200, however no cluster number selection is required for the SIMPAT algorithm. The computational time of conditional simulation for SIMPAT, FILTERSIM and our proposed method is presented in Table 1. The computing time results show that our proposed algorithm is 5 times faster than the SIMPAT algorithm and almost 2 times faster than the FILTERSIM algorithm.

The conditionally simulated realizations generated with SIMPAT, and FILTERSIM are presented in Fig. 9. Visual inspection suggests that the SWS algorithm (Fig. 6) has performed better than FILTERSIM, however has no significant difference from SIMPAT. However, the computing time of SWS is 5 times less than SIMPAT and 2 times less than the FILTERSIM algorithm. Moreover, the

channel reproduction at the top-left corner of the image is comparatively better in the proposed algorithm than in SIMPAT and FILTERSIM. In conclusion, SWS is computationally faster and provides very satisfactory results. It is important to note that FILTERSIM is producing more channels than the other methods as shown in Fig. 9(a) and (b), and Fig. 10. As a result, the data histogram is not reproduced by FILTERSIM realizations in contrast to SWS realizations as shown in Fig. 11. Having reproduced significantly more channels in the FILTERSIM realizations than the reference image also has a significant impact on the flow responses as discussed later.

4.2. Single and transport simulations

4.2.1. Incompressible two-phase flow problem

In this section, we solve an incompressible two-phase fluid flow problem. The flow of a wetting phase (i.e. water) and a non-wetting phase (i.e. oil) in a n-D (n = 1, 2 or 3) polygonal porous medium and over a time interval $[0,T]$ is described by Darcy's law and the saturation equation for each phase [55,56]. A Galerkin finite element approach is employed to resolve the flow problem [55,58]. We consider a 2D horizontal domain (100 m × 128 m) initially saturated with oil, and we used the same level of discretization for the model discretization and the geostatistical models. We injected water from the upper right corner and produced oil at the opposite
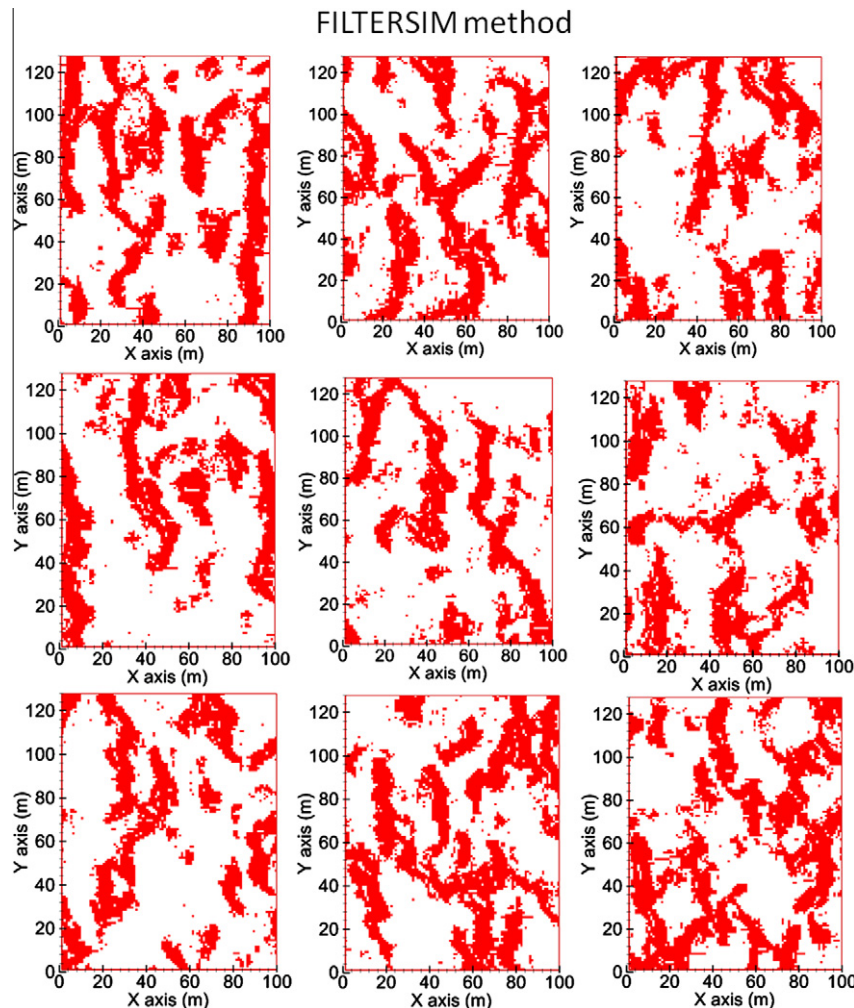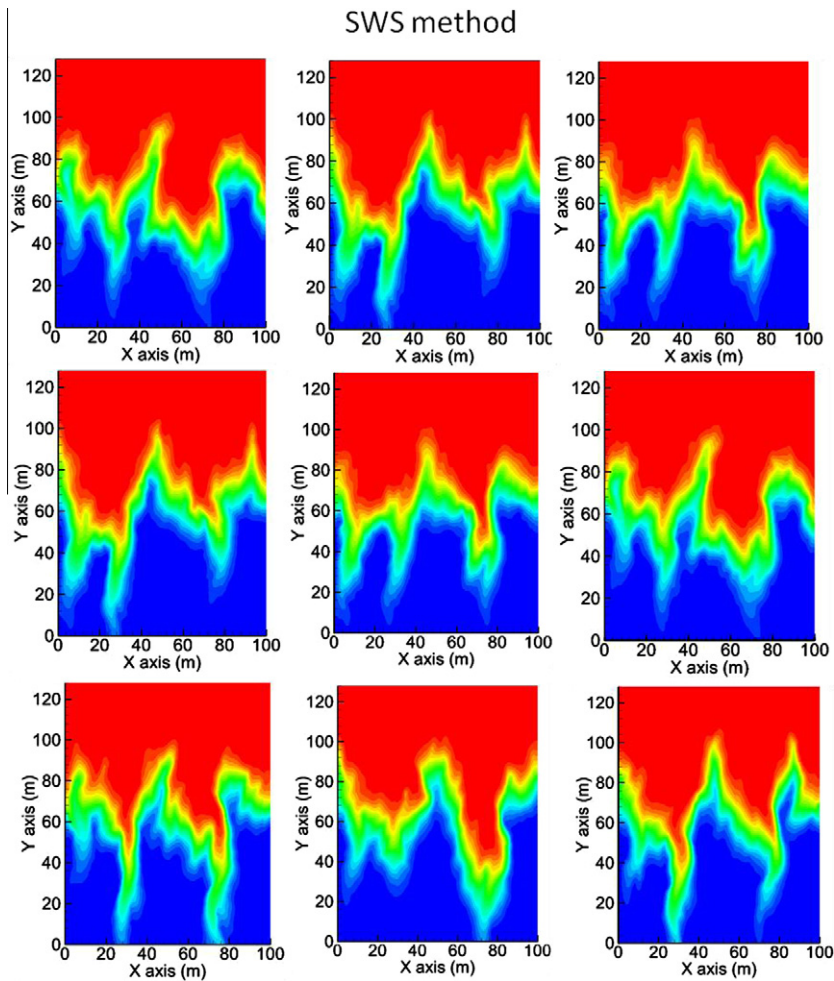

Fig. 19. Binary maps, with value 1 if K > 85% and 0 otherwise, for 9 new realizations of the FILTERSIM method simulating the spatial patterns in Fig. 18(a) using the training image in Fig. 5(b).

SWS method

Fig. 20. Solute transport simulation using the 9 new SWS realizations. Color scale represents relative solute concentration C/C_0. (For interpretation of the references to color in this figure legend, the reader is referred to the web version of this article.)

corner as shown in Fig. 12. The injection rate in pore volume (PV) is 0.1 PV/year. For simplicity, capillary pressure is neglected. The fluid and medium properties are given in Table 2.

The water saturation profiles for the reference image and for SWS and SGS realizations are all displayed in Fig. 13. In contrast to SGS, the SWS realizations and the reference image have been found to be in good agreement where very similar water saturation profiles are produced. The connected channels in the SWS realizations are very close to the connected channels in the reference image, which has the effect of conducting the injected water through the high-permeability values in a similar way. Failing to reproduce similar connected channels in the SGS realizations has the effect of obtaining different water saturation profiles, and, consequently, a different oil recovery. The oil recovery vs. PVI for both SWS and SGS realizations are plotted in Fig. 14. This figure shows a good agreement between SWS realizations and the reference image. The difference is less than 3%. However, in some SGS realizations, the oil recovery deviates 20% from the oil recovery in the reference image, clearly showing that the new SWS method presented here is superior relative to the standard SGS method.

4.2.2. Single-phase flow and solute transport problem

In this section, we solve an advective–dispersive–diffusive solute transport in a n-D (n = 1, 2 or 3) polygonal porous medium and over a time interval [0, T]. The governing equations are the Darcy's law and the solute concentration equation [34]. The

numerical simulations in this section are completed using a control volume finite element approach implemented in the HydroGeo-Sphere software [27,28,69]. We used the same model domain and gridding that is employed in the previous section. Dirichlet and Neumann boundary conditions are applied such that a solute is injected from the top where the Dirichlet boundary condition c = 1 is imposed, and lateral and bottom boundaries are Neumann conditions where dc/dn = 0. We assumed a constant head along the top and bottom Dirichlet boundaries, and lateral boundaries are no-flow Neumann boundaries. The relevant parameters used in this example are shown in Table 3.

The solute concentration profiles for the SWS and SWG realizations are shown in Fig. 15. As for the flow problem, SWS realizations are much better than SGS realizations in reproducing concentration profiles similar to the reference image concentration profile. Multiple-point connectivity of high-permeability values is relatively higher in the SWS realizations, and this may affect the solute transport behavior and the propagation of the transported plume. The average concentrations at the bottom boundary is calculated for the reference image. The SWS and SGS realizations are all displayed in Fig. 16; this figure shows that the reference solution is close to the SWS realizations average solution.

Numerical simulations are also performed using FILTERSIM realizations. However, it has been noticed that the FILTERSIM method produces significantly more channels than the other methods as discussed above. The number of channels has a big effect on

the solute propagation as shown in Fig. 17. It is important to remind readers that the objective of using a multiple-point method is not to reproduce channels but to reproduce the same number of channels as believed to be in the real images (i.e. reference images). Given that FILTERSIM is strongly reflecting the training image features, we have used a second reference image (Fig. 17(a)) that is closer to the training image shown in Fig 5(b) than the first reference image in Fig. 5(a). The same data locations are selected from the new reference image. The same solute transport problem using the same boundary conditions and input data
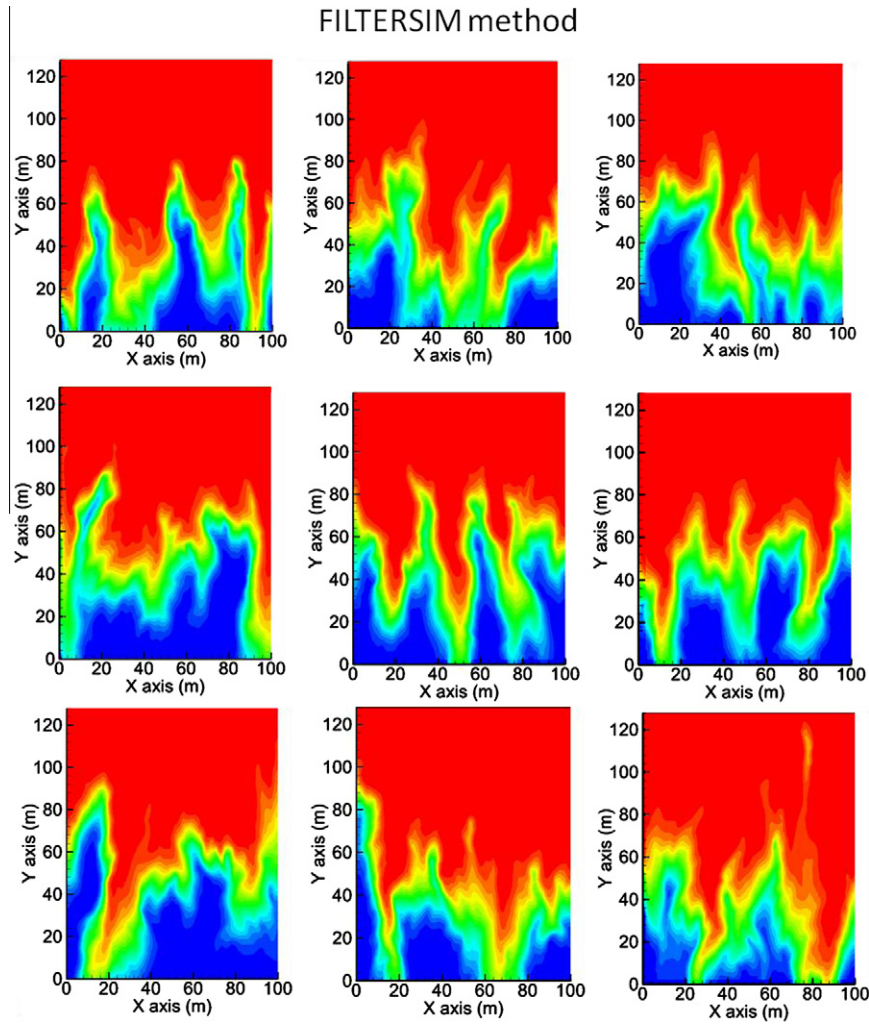

Fig. 21. Solute transport simulation using the 9 new FILTERSIM realizations. Color scale represents relative solute concentration C/C_0. (For interpretation of the references to color in this figure legend, the reader is referred to the web version of this article.)
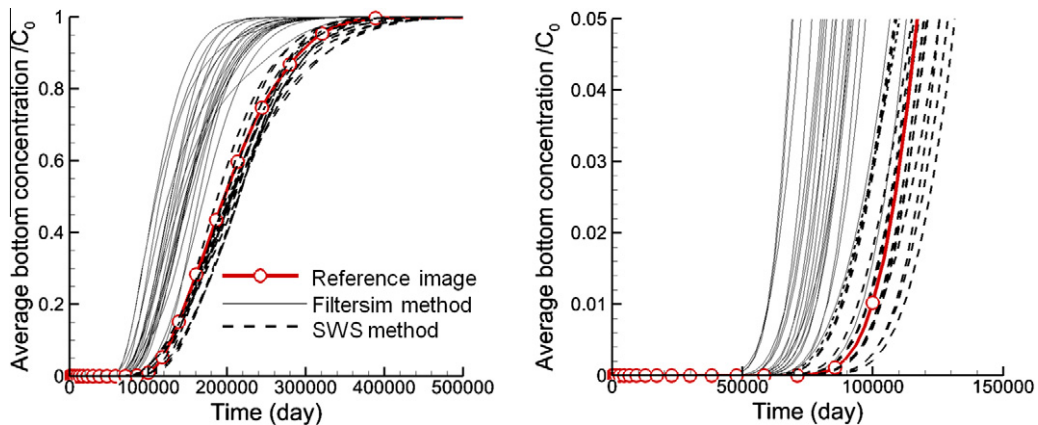

Fig. 22. Average concentration along the bottom boundary vs. time for both the proposed method SWS and FILTERSIM method realizations; the continuous line with circles refers to the concentration in the reference domain (left). A close-up is shown on the right.

is resolved using the new realizations of the SWS and FILTERSIM methods.

First, Fig. 17(b) shows the main channel configurations using a cutoff above 85%, and the corresponding reference solute concentration profiles are shown in Fig. 17(c). The main features of the SWS and FILTERSIM realizations are shown in Figs. 18 and 19, respectively.

Fig. 19 shows clearly that FILTERSIM is also producing significantly more channels in the example, confirming that FILTERSIM is a strongly training image driven algorithm. The solute transport simulation results are shown in Figs. 20 and 21. Fig. 20 shows that the results of SWS method are in good agreement with the results obtained from solving the numerical problems using the reference image as input. The FILTERSIM results are not in good agreement with the reference results. The propagation of the solute is much faster due to the number of connected channels. The average concentration at the bottom is also calculated for the SWS and FILTSE-RIM results and is shown in Fig. 22. This figure shows again the effects of over connected channels produced by the FILTERSIM method on the simulations.

All the results presented above demonstrate that flow and transport simulations based on SWS simulations are dominated by appropriate and accurate results reproduced by the level of connectivity of the channels. The SGS and FILTERSIM realizations have the same effect on the simulations; that is to reproduce very different results as they should be.

5. Conclusions

In this paper, a Sequential Wavelet-based Simulation (SWS) method is employed to represent geological heterogeneity. The generated pattern database from the training image is classified using the scaling image of the wavelet decomposed patterns. The scaling image of the optimally selected scale helps to reduce the computational time of the pattern database classification. The performance of the proposed SWS method was compared with two other multi-point simulation algorithms, FILTERSIM and SIMPAT. The results show that the SWS method is computationally faster than FILTERSIM and SIMPAT and that the simulated realizations are satisfactory. SWS, the sequential Gaussian simulation (SGS), and FILTERSIM methods are compared by illustrating their effects on underground flow and transport. The results presented showed (a) a good reproduction of data characteristics, i.e. low- and high-order statistics, obtained by SWS realizations; (b) a more appropriate connectivity, in the high-K values, obtained in SWS realizations, and a better agreement with the reference image than with SGS and FILTERSIM; (c) a more consistent and stable behavior of the water flow using SWS realizations; (d) a more accurate reproduction of oil recoveries by SWS realizations compared to the recoveries in the reference image, as opposed to the approximate 20% error that characterizes the SGS realizations; and (e) an agreement between reference and SWS solutions for solute concentration profiles.

Acknowledgments

References

[1] Ababou R, McLaughlin D, Gelhar LW, Tompson AFB. Numerical simulation of three dimensional saturated flow in randomly heterogeneous porous media. Transp Porous Media 1989;4:549–66.

[2] Alabert FG, Aquitaine E, Modot V. Stochastic models of reservoir heterogeneity: impact on connectivity and average permeabilities. SPE 1992;24893:355–70.

[3] Anderson MP. Universal scaling of hydraulic conductivities and dispersivities in geologic media – comment. Water Resour Res 1991;27:1381–2.

[4] Arpat G, Caers J. Conditional simulation with patterns. Math Geol 2007;39(2):177–203.

[5] Arpat G. Sequential simulation with patterns. PhD thesis, Stanford University, 2004.

[6] Ballio F, Guadagnini A. Convergence assessment of numerical Monte Carlo simulations in groundwater hydrology. Water Resour Res 2004;40(4). http://dx.doi.org/10.1029/2003WR002876.

[7] Bear J. Dynamics of fluids in porous media. New York: Elsevier; 1972. p. 784.

[8] Boucher A. Considering complex training images with search tree partitioning. Comput Geosci 2009;35:1151–8.

[9] Caers J. Petroleum geostatistics. Huston: SPE – Pennwell Books; 2005.

[10] Chatterjee S, Dimitrakopoulos R, Mustapha H. Dimensional reduction of pattern-based simulation using wavelet analysis. Math Geosci 2012. http://dx.doi.org/10.1007/s11004-012-9387-4.

[11] Chilès JP, Delfiner P. Geostatistics: modeling spatial uncertainty. New York: Wiley; 1999.

[12] Chugunova TL, Hu LY. Multiple-point simulations constrained by continuous auxiliary data. Math Geosci 2008;40:133–46.

[13] Cressie NA. Statistics for spatial data. New York: Wiley; 1993.

[14] Daly C. Higher order models using entropy, Markov random fields and sequential simulation. In: Geostatistics Banff. Springer; 2004. p. 215–25.

[15] David M. Geostatistical ore reserve estimation. Amsterdam: Elesevier; 1977.

[16] David M. Handbook of applied advanced geostatistical ore reserve estimation. Amsterdam: Elsevier; 1988.

[17] Daubechies I. Ten lectures on wavelets. Philadelphia: SIAM; 1992.

[18] de Marsily G, Delay F, Teles F, Schafmeister MT. Some current methods to represent the heterogeneity of natural media in hydrogeology. Hydrogeol J 1998;6:115–30.

[19] Desbarats AJ. Macrodispersion in sand-shale sequences. Water Resour Res 1990;26:153–63.

[20] Desbarats AJ, Srivastava RM. Geostatistical characterization of groundwater flow parameters in a simulated aquifer. Water Resour Res 1991;27:687–98.

[21] Deutsch CV, Journel AG. GSLIB geostatistical software library and user's guide. New York: Oxford University Press; 1998.

[22] Dimitrakopoulos R, Mustapha H, Gloaguen E. High-order statistics of spatial random fields: exploring spatial cumulants for modeling complex non-gaussian and non-linear phenomena. Math Geosci 2010;42:65–99.

[23] Ding C, He X. K-means clustering via principal component analysis. In: Proceedings of interantional conference on machine learning (ICML 2004), 2004, p. 225–32.

[24] Feyen L, Gorellick S. Reliable groundwater management in hydroecologically sensitive areas. Water Resour Res 2004;40(7). http://dx.doi.org/10.1029/2003WR003003.

[25] Fogg GE. Groundwater flow and sand body interconnectedness in a thick multiple-aquifer system. Water Resour Res 1986;22:679–94.

[26] Fogg GE, Carle SF, Green C. Connected-network paradigm for the alluvial aquifer system. In: Zhang D, Winter CL, editors. Theory, modeling, and field investigation in hydrogeology: a special volume in honor of Shlomo P. Neuman's 60th birthday. Boulder (Co), Geological Society of America Special Paper 348, 2000, p. 25–42.

[27] Forsyth PA, Simpson RB. A two phase, two component model for natural convection in a porous medium. Int J Numer Methods Fluids 1991;12:655–82.

[28] Forsyth PA. A control volume finite element approach to NAPL groundwater contamination. SIAM J Sci Stat Comput 1991;12:1029–57.

[29] Gloaguen E, Dimitrakopoulos R. Two dimensional conditional simulation based on the wavelet decomposition of training images. Math Geosci 2009;41(7):679–701.

[30] Gomez-Hernandez JJ, Wen XH. To be or not to be multi-Gaussian? A reflection on stochastic hydrogeology. Adv Water Resour 1998;21:47–61.

[31] Goovaerts P. Geostatistics for natural resources evaluation. Oxford: New York; 1998.

[32] Goshtasby A, Gage SH, Bartholic JF. A two-stage cross-correlation approach to template matching. IEEE Trans Pattern Anal Mach Intell 1984;6(3):374–8.

[33] Gotway CA, Rutherford BM. Stochastic simulation for imaging spatial uncertainty: comparison and evaluation of available algorithms. In: Armstrong M, Dowd PA, editors. Geostatistical simulation workshop: geostatistical simulations: proceedings of the geostatistical simulation workshop. Fontainebleau, France, Boston: Kluwer Academic Publishers; 1994. p. 1–21.

[34] Graf T, Therrien R. Variable-density groundwater flow and solute transport in porous media containing nonuniform discrete fractures. Adv Water Resour 2005;28:1351–67.

[35] Guardiano J, Srivastava RM. Multivariate geostatistics: beyond bivariate moments. In: Soares A, editor. Geostatics Tróia '92, vol. 1. Dordrecht: Kluwer; 1993. p. 33–144.

[36] Hartigan JA, Wong MA. Algorithm AS 136: a K-means clustering algorithm. J R Stat Soc, Ser C (Appl Stat) 1979;28(1):100–8.

[37] Honarkhah M, Caers J. Stochastic simulation of patterns using distance-based pattern modelling. Math Geosci 2010;42:487–517.

[38] Jones A, Doyle J, Jacobsen T, Kjonsvik D. Which subseismic heterogeneities influence waterflood performance – a case study of a low net-to-gross fluvial reservoir. In: de Hann HJ, editor. New developments in improved oil recovery, vol. 84. Geological Society of America Special Publication; 1995. p. 5–18.

[39] Journel AG. Deterministic geostatistics: a new visit. In: Baafy E, Shofield N, editors. Geostatistics Woolongong. Dordrecht: Kluwer; 1997. p. 213–24.

[40] Journel AG, Huijbregts ChJ. Mining geostatistics. New York: Academic Press Inc.; 1978.

[41] Journel AG, Alabert F. Non-Gaussian data expansion in the earth sciences. TERRA Nova 1989;1:123–34.

[42] Journel AG, Deutsch CV. Entropy and spatial disorder. Math Geol 1993;25:329–55.

[43] Juanes R, MacMinn CW, Szulczewski ML. The footprint of the CO2 plume during carbon dioxide storage in saline aquifers: storage efficiency for capillary trapping at the basin scale. Transp Porous Media 2009;82:19–30. http://dx.doi.org/10.1007/s11242-009-9420-3.

[44] Kitanidis PK. Introduction to geostatistics – applications in hydrogeology. New York: Cambridge University Press; 1997.

[45] Kuglin C, Hines D. The phase correlation image alignment method. In: Proceedings of the international conference on cybernetics and society, 1975, p. 163–5.

[46] Lee SY, Steven FC, Graham EF. Geologic heterogeneity and a comparison of two geostatistical models: sequential Gaussian and transition probability-based geostatistical simulation. Adv Water Resour 2007;30:1914–32.

[47] MacMinn CW, Juanes R. Post-injection spreading and trapping of CO2 in saline aquifers: Impact of the plume shape at the end of injection. Comput Geosci 2009;13:483–91. http://dx.doi.org/10.1007/s10596-009-9147-9.

[48] MacQueen JB. Some methods for classification and analysis of multivariate observations. Proceedings of 5th Berkeley symposium on mathematical statistics and probability, vol. 1. Berkeley: University of California Press; 1967. p. 281–97.

[49] Mallat S. A wavelet tour of signal processing. San Diego, CA: Academic Press; 1998.

[50] Mao S, Journel AG. Generation of a reference petrophysical and seismic 3D data set. In: The Stanford V reservoir, in Stanford Center for Reservoir Forecasting Annual Meeting, 1999. Available from: <http://ekofisk.stanford.edu/SCRF.html>.

[51] Matheron G. The theory of regionalized variables and its applications. In: Cahier du Centre de Morphologie Mathematique, No. 5, Fointanebleau, 1971.

[52] Mirowski PW, Trtzlaff DM, Davies RC, McCormick DS, Williams N, Signer C. Stationary scores on training images for multipoint geostatistics. Math Geosci 2008;41:447–74.

[53] Moreno L, Tsang CF. Flow channeling in strongly heterogeneous porous media – a numerical study. Water Resour Res 1994;30:1421–30.

[54] Mustapha H. Simulation numérique de lécoulement dans des milieux fracturés tridimensionnels. Thése de Doctorat, Université de Rennes 1, 2005. Available from: <http://www.irisa.fr/centredoc/publis/theses#2005>.

[55] Mustapha H, Dimitrakopoulos R. Discretizing two-dimensional complex fractured fields for incompressible two-phase flow. Int J Numer Methods Fluids 2009. http://dx.doi.org/10.1002/fld.2197.

[56] Mustapha H, Dimitrakopoulos R. A new approach for geological pattern recognition using high-order spatial cumulants. Comput Geosci 2010;36:313–34.

[57] Mustapha H, Dimitrakopoulos R. Conditional simulations of complex geological patterns using high-order multi-point spatial cumulants. Math Geosci 2010;42(5):455–73.

[58] Mustapha H, Dimitrakopoulos R, Graf T, Firoozabadi A. An efficient method for discretizing 3D fractured media for subsurface flow and transport simulations. Int J Numer Methods Fluids 2011;67:651–70.

[59] Mustapha H, Chatterjee S, Dimitrakopoulos R. Geologic heterogeneity representation using high-order spatial cumulants for subsurface flow and transport simulations. Water Resour Res 2011;47:W08536. http://dx.doi.org/10.1029/2010WR009515.

[60] Quddus A, Gabbouj M. Wavelet-based corner detection technique using optimal scale. Pattern Recognit Lett 2002;23:215–20.

[61] Remy N, Boucher A, Wu J. Applied geostatistics with SGeMS: a users's guide. New York: Cambridge University Press; 2009.

[62] Scheibe TD, Murray CJ. Simulation of geologic patterns: A comparison of stochastic simulation techniques for groundwater transport modeling. In: Fraser GS, Davis JM, editors. Hydrogeologic models of sedimentary aquifers: Tulsa(Okla): SEPM (Society of Economic Paleontologists and Mineralogists), Concepts in Hydrogeology and Environmental Geology, vol. 1; 1998. 188 p.

[63] Scheidt C, Caers J. Representing spatial uncertainty using distances and kernels. Math Geosci 2009;41:397–419.

[64] Smith L, Schwartz FW. Mass transport, 2. Analysis of uncertainty in prediction. Water Resour Res 1981;17:351–69.

[65] Smith L, Freeze RA. Stochastic analysis of steady state groundwater flow in a bounded domain, 1. One-dimensional simulation. Water Resour Res 1979;15:521–8.

[66] Smith L, Freeze RA. Stochastic analysis of steady state groundwater flow in a bounded domain, 2 Two-dimensional simulation. Water Resour Res 1979;15:1543–59.

[67] Strebelle S. Conditional simulation of complex geological structures using multiple point statistics. Math Geosci 2002;34:1–22.

[68] Sunderrajan K, Journel AG. Spatial connectivity: from variograms to multiple-point measures. Math Geol 2004;35:915–25.

[69] Therrien R, McLaren RG, Sudicky EA. HydroGeoSphere – a three-dimensional numerical model describing fully-integrated subsurface and surface flow and solute transport (Draft ed.). Groundwater Simulations Group, University of Waterloo, 2009. <http://www.science.uwaterloo.ca/~mclaren/public/hydrosphere.pdf>.

[70] Therrien R, Sudicky EA. Three-dimensional analysis of variably saturated flow and solute transport in discretely fractured porous media. J Contam Hydrol 1996;23:1–44.

[71] Tibshirani R, Walther G, Hastie T. Estimating the number of clusters in a data set via the gap statistic. J R Statist Soc B 2001;63(2):411–23.

[72] Tjelmeland H. Markov random fields with higher order interactions. Scand J Stat 1998;25:415–33.

[73] Tjelmeland H, Eidsvik J. Directional Metropolis: hastings updates for conditionals with nonlinear likelihoods. Geostatistics Banff 2004, vol. 1. p. 95–104.

[74] Wagner BJ, Gorelick SM. Reliable aquifer remediation in the presence of spatial variable hydraulic conductivity: from data to design. Water Resour Res 1989;25:2211–25.

[75] Webster R, Oliver MA. Geostatistics for environmental scientists. London: Wiley; 2007.

[76] Wen XH, Kung C. Stochastic simulation of solute transport in heterogeneous formations: a comparison of parametric and nonparametric geostatistical approaches. Ground Water 1993;31:953–65.

[77] Wen XH, Gomez-Hernandez J. Numerical modeling of macrodispersion in heterogeneous media: a comparison of multi-Gaussian and nonmulti-Gaussian models. J Contam Hydrol 1998;30:129–56.

[78] Western AW, Bloschl G, Grayson RB. Toward capturing hydrologically significant connectivity in spatial patterns. Water Resour Res 2001;37:83–97.

[79] Wu J, Boucher A, Zhang T. SGeMS code for pattern simulation of continuous and categorical variables: FILTERSIM. Comput Geosci 2008;34:1863–76.

[80] Zhang T, Switzer P, Journel AG. Filter-based classification of training image patterns for spatial simulation. Math Geosci 2006;38:63–80.

[81] Zinn B, Harvey CF. When good statistical models of aquifer heterogeneity go bad: a comparison of flow, dispersion, and mass transfer in connected and multivariate gaussian hydraulic conductivity fields. Water Resour Res 2003;39. http://dx.doi.org/10.1029/2001WR001146.